

A new *ab initio* modeling scheme for ion self-diffusion coefficient applied for ε -Cu₃Sn phase of Cu-Sn alloy

Tom Ichibha^{1,*}, Genki Prayogo², Kenta Hongo^{3,4,5,6}, and Ryo Maezono^{1,6}

¹ School of Information Science, JAIST, Asahidai 1-1, Nomi, Ishikawa, 923-1292, Japan

² School of Materials Science, JAIST, Asahidai 1-1, Nomi, Ishikawa, 923-1292, Japan

³ Research Center for Advanced Computing Infrastructure,
JAIST, Asahidai 1-1, Nomi, Ishikawa 923-1292, Japan

⁴ Center for Materials Research by Information Integration,
Research and Services Division of Materials Data and Integrated System,
National Institute for Materials Science, Tsukuba 305-0047, Japan

⁵ PRESTO, Japan Science and Technology Agency, 4-1-8 Honcho, Kawaguchi-shi, Saitama 322-0012, Japan

⁶ Computational Engineering Applications Unit, RIKEN, 2-1 Hirosawa, Wako, Saitama 351-0198, Japan and

* ichibha@icloud.com
(Dated: March 16, 2022)

We present a new modeling scheme for ion self-diffusion coefficient, which broadens the applicable scope of *ab initio* approach. The essential concepts of the scheme are ‘domain division’ and ‘coarse graining’ of the diffusion network based on the barrier energies predicted by the *ab initio* calculation. The scheme was applied to evaluate Cu ion self-diffusion coefficient in ε -Cu₃Sn phase of Cu-Sn alloy, which is a typical system having long-range periodicity. The model constructed with the scheme successfully reproduces the experimental values in a wide temperature range.

INTRODUCTION

Ion diffusion attracts the broad interests of the material researchers because it dominates the various important phenomena in the solid: corrosion, monotectoid, fracture, degradation and so on. In order to elucidate the microscopic mechanism of the ion diffusion, *ab initio* calculation is one of the most powerful tools. For example, it can evaluate the barrier energy of the diffusion route with such techniques as nudged elastic band (NEB) method[1]. Even the ion self-diffusion coefficient [2] has been reported theoretically, [3–8] combining the *ab initio* predictions with modeling schemes such as five-frequency model.[9–11] These theoretical works however target just simplest crystals mainly due to the following two difficulties.

First, the system appearing in the practical situation often requires a large size of unitcell because of long-range periodicity, which makes the calculation expensive, otherwise infeasible. Such a problem is especially severe, for example, when optimizing the ion path through the diffusion route using NEB method because it requires a lot of force-field calculations for a number of structures. Secondly, it is very hard to count up and evaluate all of the ion diffusion processes in most cases so the application range of *ab initio* approach is limited within just simplest systems.

To overcome the difficulties, we introduced a couple of novel concepts, which significantly simplifies the diffusion network based on the barrier energies. First, suppose to classify the diffusion routes according to the barrier energies into the three groups *I-III* as the energies ordering like $\Delta E_I \ll \Delta E_{II} \ll \Delta E_{III}$. Since the barrier energy exponentially contributes the diffusion coefficient (*i.e.* Boltzmann factor), the diffusion routes (III) can be excluded from the diffusion

network. Then, the network may be divided into several disjunct domains and the expensive calculation for the large unit-cell can be replaced by the several cheaper calculations for the small domains. This is a concept to solve the first difficulty. In addition, the diffusion network in each of the domains may be further simplified by coarse-graining: The vacancy can move almost freely through the diffusion routes (I) compared with moving through the routes (II), so the ion sites connected by the routes (I) can be represented by just a site. Eventually, the diffusion network falls into coarse-grained one with the representative sites, where it is much easier to count up the diffusion processes.

We established a modeling scheme based on the above concepts for the example of the Cu ion self-diffusion coefficient in ε -Cu₃Sn phase of Cu-Sn alloy. This is a typical system having long-range periodicity and there is abundant experimental data for the Cu self-diffusion coefficient. [12–17] From simulation side, classical molecular dynamics (MD) was applied[18] but it overestimated the experimental values by a digit. On the other hand, the model constructed with our scheme successfully reproduced them in a wide temperature range.

This paper consists of the following sections: In the next section (Formalism), we introduce the equations for the physical quantities relevant to the ion diffusion and also define the technical terms and the notation rules. In the 3rd section (Domain division), we explain how to divide the diffusion network into the multiple types of the simple domains, based on the barrier energies. In the 4th section (Details and results of *ab initio* calculation), we present the predictions for the quantities (ex. barrier energy, vacancy formation energy) calculated with the density functional calculation. The details of the calculations are also given here. In the 5th section (Coarse graining), we discuss how to represent the multiple ion sites with

just a site and coarse-grain the diffusion network, based on the barrier energies. In the 6th section (Formula of self-diffusion coefficient), We discuss how to model the self-diffusion coefficient when there are two or more types of diffusion routes. In the 7th section (Evaluation of correlation factor), it is deeply discussed how to count up the possible diffusion processes in the simplified diffusion network and evaluate the correlation factor with some approximations. In the 8th section (Results and discussions), the validity of the model constructed with our scheme is discussed, compared with the experimental values for the self-diffusion coefficient or the correlation factor for ideal hexagonal 2-dimensional lattice. In the 9th section (Summary and prospects), we summarize this paper and refer to the advantage of our scheme from *ab initio* MD.

FORMALISM

The self-diffusion coefficient $D(w)$ represents the macroscopic ion flow in a direction w driven by self-diffusion. $D(w)$ is obtained by evaluating the ion jump, which is a minimum process of the ion diffusion. We index the diffusion routes connecting to a site with j and define $\theta_j(w)$ as the angle of the ion jump thorough route j from direction w . We also define D_j^* as the angle-independent contribution of the ion jump to the self-diffusion coefficient (explained in the next paragraph) and the self-diffusion coefficient $D(w)$ is evaluated from the following equation:[19]

$$D(w) = \sum_j \frac{1}{2} D_j^* \cos^2 \theta_j(w). \quad (1)$$

D_j^* consists of the four quantities appeared in the following equation (index j is omitted): [19]

$$D^* = d^2 \cdot f \cdot C_v \cdot \eta. \quad (2)$$

d is the distance of the diffusion route. C_v is the vacancy formation rate given as the Boltzmann factor of the vacancy formation energy ΔE_{vac} . η is the jump rate depending on the barrier energy $\Delta E_{\text{barrier}}$ and the vibration frequency ν of the attentional ion (tracer) in the jump direction:

$$\eta = \nu \cdot \exp(-\Delta E_{\text{barrier}}/k_B T). \quad (3)$$

f is called correlation factor and explained in the next paragraph. The evaluation of the vacancy formation energy ΔE_{vac} needs the chemical potential μ_{Cu} of Cu ion. We calculated it for face-centered Cu mono-crystal and got the ΔE_{vac} from the following equation:

$$\Delta E_{\text{vac}} = E_{\text{vac}} - E_{\text{perfect}} + \mu_{\text{Cu}}. \quad (4)$$

Here, E_{perfect} is the total energy of perfect crystal and E_{vac} is that of the crystal including a vacancy defect.

The evaluation of the correlation factor f is the most awful part for the modeling of self-diffusion coefficient. The factor reflects the position exchanges sequentially occurring between the vacancy and the tracer: After the tracer jumping via

the vacancy, it is at the behind of the tracer. Thus, the vacancy tends to pull back the tracer at the next ion jump around the reverse direction of the ion jump. In addition, such a pull-back can occur again and again after the 1st pull-back, always around the reverse direction of the preceding tracer move. The correlation factor f represents how much the sequential pull-backs affect the self-diffusion coefficient in total. Since the 1st pull-back denying the tracer jump has the largest contribution to the correlation factor, it always reduces D_j^* (i.e. $0 \leq f \leq 1$).

To evaluate correlation factor, we have to count up all of the vacancy tracks from the one to the next position exchange between the tracer and the vacancy. This is the identity of the first difficulty. The contribution from each of the pull-backs to the self-diffusion coefficient is given as average cosine:

$$\langle \cos \theta \rangle^{(n)} = \sum_k^Z P_k \cos \theta_k. \quad (5)$$

Here, P_k is the sum of the realization probability of the vacancy tracks causing the pull-back from site k . θ_k is the angle of the tracer move at the pull-back from the preceding tracer move. We also define n th-order average cosine $\langle \cos \theta \rangle^{(n)}$, which represents how much the first ion jump is denied by the n times pull-backs in average. The correlation factor f consists of them as the following equation:

$$f = 1 + 2 \sum_{n=1}^{\infty} \langle \cos \theta \rangle^{(n)}. \quad (6)$$

‘ $(n+1)$ times of pull-back’ is interpreted as one extra pull-back occurring after ‘ n times of pull-back’ so $\langle \cos \theta \rangle^{(n)}$ is given as

$$\langle \cos \theta \rangle^{(n+1)} = \langle \cos \theta \rangle^{(n)} \langle \cos \theta \rangle. \quad (7)$$

Especially when there is only one diffusion route, [20] the following relationship is hold:[19]

$$\langle \cos \theta \rangle^{(n)} = \langle \cos \theta \rangle^n. \quad (8)$$

This equation is generalized for multiple diffusion routes later in section (formula of correlation factor).

DOMAIN DIVISION

ε -Cu₃Sn phase has, it is reported, long-range periodic structure (Fig. 1a). It has been recognized that the structure consists of the unitcells of Cu₃Ti-type structure with shifted by 1/2 in fractional coordinate along a -axis, every $M/2$ unitcells lining up along b -axis (Fig. 1a). The various periodicities M are reported experimentally as the even numbers from 2 to 12. [21, 22] Based on the *ab initio* predictions, it is newly found that the ion jump though the diffusion route passing between the Sn sites hardly contributes to the self-diffusion because their barrier energies are much higher than the others. After excluding these routes from the diffusion network, it is divided into the two types of simple domains, Cu₃Ti-type and D0₁₉-type, as shown in Fig. 1b. The both domains exist in

the ratio of $(M-2):2$ so the self-diffusion coefficient of the target phase is given as the weighted average of them with the existing ratio:

$$D_{\varepsilon-\text{Cu}_3\text{Sn}} = \frac{M-2}{M} D_{\text{Cu}_3\text{Ti}} + \frac{2}{M} D_{\text{D0}_{19}}. \quad (9)$$

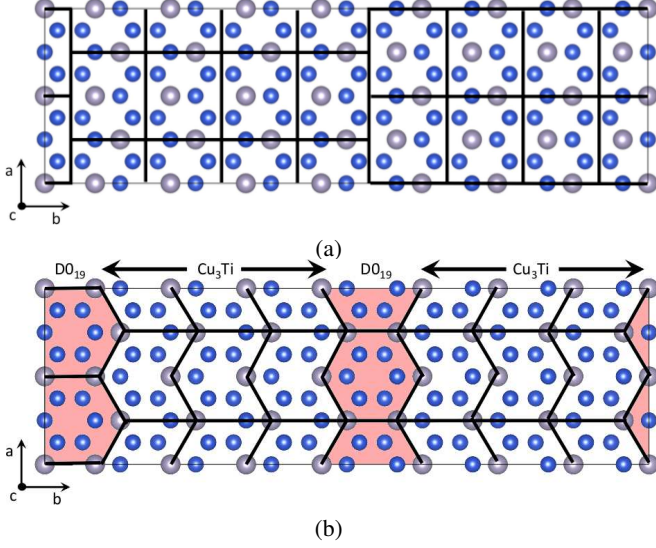


FIG. 1. The crystal structure of ε - Cu_3Sn [21] The blue balls represent Cu ions and the gray balls do Sn ions. Figure (a) shows the conventional interpretation for the long-range periodic structure. Cu_3Ti -type unitcell (surrounded by thick line) is shifted by $1/2$ period along a direction every $M/2$ (M : periodicity) unitcells lining up along b direction. Figure (b) shows our new interpretation. $(M-2)/2$ unitcells of Cu_3Ti -type structure and one D0_{19} -type unitcell appear periodically along b direction. The pictures are made with VESTA.[23]

DETAILS AND RESULTS OF *AB INITIO* CALCULATION

We employed $2 \times 2 \times 2$ supercell for both Cu_3Ti -type and D0_{19} -type domains to reduce the spurious interaction between the vacancies. The lattice parameters are fixed at the experimental values.[21] We used VASP[24] for the density functional calculation to evaluate the physical quantities. The barrier energies are evaluated with climbing-nudged elastic band (c-NEB) method [1] implemented in VASP. [24] c-NEB needs the interpolated structures between the both edges of the diffusion path as inputs and optimizes them with connected by the virtual springs. c-NEB guarantees that one of the structures is positioned at the exact saddle point of the given potential surface, in which c-NEB is superior to the original NEB method.[25] We prepared 15 interpolated structures and set the spring coefficient as $5 \text{ eV}/\text{\AA}^2$. We used PBE functional [26] and PAW pseudopotentials provided in VASP[27] for all of the calculations. We determined the cut-off energy and k-mesh for the total energy to be converged within 0.5 kJ/unitcell for the both Cu_3Ti -type and D0_{19} -type domains. We calculated the vibrational frequency of the tracer

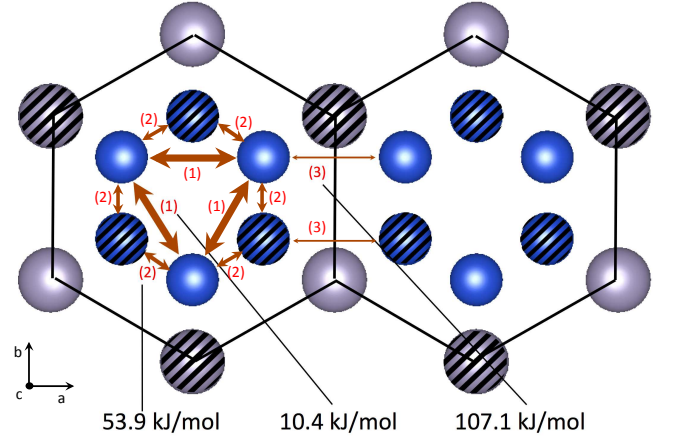


FIG. 2. The diffusion routes and the barrier energies of Cu ion in D0_{19} -type domain. The diffusion routes are shown as the two-way arrows with the values of the barrier energies. The blue balls represent Cu ions and the gray balls do Sn ions. The hatched balls are located on $c=1/2$ plane and the unhatched ones are on $c=0, 1$ plane in fractional coordinate. The ion diffusion occurs in the 1-dimensional tubes partitioned by the thick black lines, since the energy barriers of the route 3 across the lines are much higher than the others. This picture is made with VESTA[23].

in the jump direction with the harmonic approximation of the potential surface.

The diffusion routes in D0_{19} -type (Cu_3Ti -type) domain is shown in Fig. 2 (Fig. 3). The diffusion barriers for D0_{19} -type domain are written in the figure. Those for the Cu_3Ti -type domain are written in Tab. I with the vibrational frequencies ν in the jump direction and jump rate η at 300 K and 423 K. It can be observed from the table that the route 3 of D0_{19} -type domain and the route 6, 6' of Cu_3Ti -type have the highest barrier energies, which is the ground of the domain division of the diffusion network. D0_{19} -type domain has only one type of Cu site and the vacancy formation energy was calculated as 16.60 kJ/mol . Cu_3Ti -type domain has two types of Cu site denoted by 'top' and 'base' in Fig. 3. The vacancy formation energies are calculated as 25.94 kJ/mol for 'top' and 21.71 kJ/mol for 'base'.

COARSE GRAINING

In the structure of D0_{19} -type domain, the hexagonal tubes consisting of Cu sites surrounded in the lines connecting Sn sites. Each of the tubes consists of the laminated Cu ions arranged in the triangle shape located in the different ab -planes by $1/2$ in fractional coordination (hatched and unhatched sites). Since the barrier energy of route 3 connecting the two tubes is much higher than the others, the ions diffuse in each of the independent tubes. In addition, route 1 has much lower barrier energy than route 2 so the vacancy can move inside of the triangle through route 1 much more easily than moving across the triangle through route 2. Therefore, it

TABLE I. The list of the physical quantities relevant to the ion diffusion in Cu_3Ti -type domain. The indices i correspond to the ones of the diffusion routes shown in Fig. 3. ΔE_i is the energy barrier, ν_i is the vibration frequency towards the jump direction, and η_i is the ion jump frequencies at 300 K and 423 K.

Path i	ΔE_i [kJ/mol]	ν_i [sec. ⁻¹]	η_i (300 K) [sec. ⁻¹]	η_i (423 K) [sec. ⁻¹]
1	54.59	3.675×10^{12}	1.151×10^3	6.680×10^5
1'	58.82	3.575×10^{12}	2.049×10^2	1.948×10^5
2	69.65	4.152×10^{12}	3.096×10^0	1.041×10^4
3	21.69	3.155×10^{12}	5.288×10^8	6.625×10^9
3'	25.91	2.542×10^{12}	7.828×10^7	1.605×10^9
4	60.19	4.138×10^{12}	1.369×10^2	1.527×10^5
5	51.60	3.618×10^{12}	3.748×10^3	1.536×10^6
6	99.44	—	—	—
6'	103.66	—	—	—

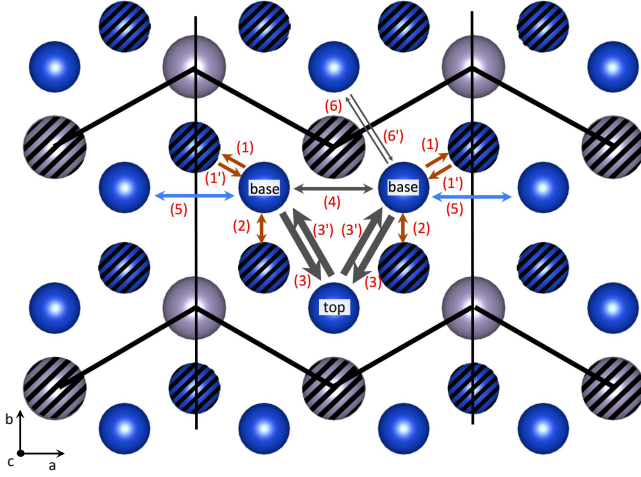


FIG. 3. The diffusion routes of Cu ion in Cu_3Ti -type domain. The blue balls represent Cu ions and gray balls do Sn ions. The hatched balls are located on $c=1/2$ plane and the unhatched ones are on $c=0, 1$ plane in fractional coordinate. The diffusion routes are shown as the red arrows (1,1',2) and blue ones (5) and they are named route \tilde{c} and a respectively. The both-side arrow represents that the ion jumps in normal and reverse directions are equivalent. The ion diffusion occurs in the 2-dimensional layers partitioned by the thick black lines, since the energy barriers of the route 6,6' across the lines are much higher than the others. This picture is drawn with VESTA[23].

would be possible to represent the triangle with just a site, and the diffusion network is coarse-grained into the 1-dimensional one long c -axis composed of the representative sites, named rep-site (a schematic picture given in Fig. 4). The correlation factor of 1-dimensional diffusion is known to be zero in the textbook[19] and hence

$$D_{\text{D0}_{19}} = 0. \quad (10)$$

The diffusion network of Cu_3Ti -type domain can be also coarse-grained with the same analogy yet into the 2-dimensional one: The barrier energy of route 6,6f is much higher than the others so the ion diffusion occurs in the layers

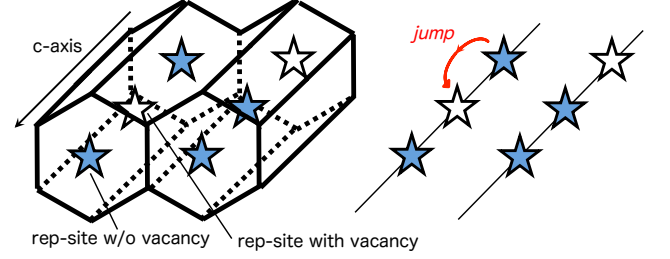


FIG. 4. The left figure shows the coarse-grained diffusion network of D0_{19} -type domains with the rep-sites. The star represents rep-site and the open one includes the vacancy. Since the tracer seldomly jumps perpendicular to c -axis, the diffusion network is almost 1-dimensional.

partitioned by the thick lines written in Fig. 3. In addition, the barrier energies of route 3,3f are much lower than the others, so the three sites connected by route 3,3f can be represented by a rep-site. The vacancy formation rate of the rep-site would reasonably be evaluated as

$$C_v^{(\text{rep})} = C_v^{(\text{top})} + 2C_v^{(\text{base})}. \quad (11)$$

After the coarse-graining with using a rep-site, the diffusion network becomes the 2-dimensional one consisting of two types of diffusion routes a , \tilde{c} shown in Fig. 5. (Noted that route a is parallel to a -axis but route \tilde{c} deviates from c -axis.) Route a consists of route 5 and route \tilde{c} consists of route 1,1',2 so the jump rates through routes a , \tilde{c} can be given as:

$$C_v^{(\text{rep})} \cdot \eta_a = C_v^{(\text{base})} \cdot \eta_5, \quad (12)$$

$$C_v^{(\text{rep})} \cdot \eta_{\tilde{c}} = C_v^{(\text{top})} \cdot \eta_1 + C_v^{(\text{base})} \cdot (\eta_{1'} + \eta_2). \quad (13)$$

We define $\gamma^{(\text{top})}$, $\gamma^{(\text{base})}$ as:

$$\gamma^{(\text{top})} \equiv C_v^{(\text{top})} / C_v^{(\text{rep})}, \quad \gamma^{(\text{base})} \equiv C_v^{(\text{base})} / C_v^{(\text{rep})}. \quad (14)$$

and substitute $\gamma^{(\text{top})}$, $\gamma^{(\text{base})}$ into eq. (12),(13). Then, we can get the effective jump rates η_a , $\eta_{\tilde{c}}$ as:

$$\eta_a = \gamma^{(\text{base})} \eta_5, \quad \eta_{\tilde{c}} = \gamma^{(\text{top})} \eta_1 + \gamma^{(\text{base})} (\eta_{1'} + \eta_2). \quad (15)$$

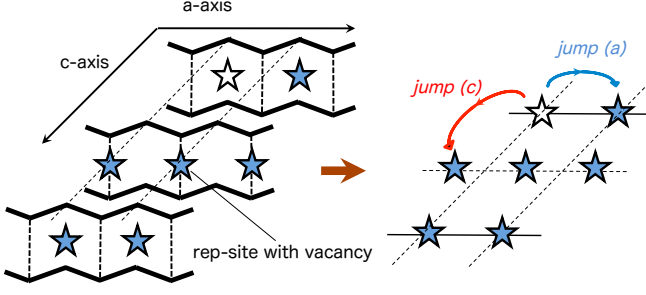


FIG. 5. The left figure shows the coarse-grained diffusion network of Cu_3Ti -type domain with the rep-sites. The star represents rep-site and the open one includes the vacancy. Since the tracer seldomly jumps perpendicular to ac -plane, the diffusion network is almost 2-dimensional. The rep-sites are connected with two types of routes name route a and \tilde{c} . Route a is parallel to a -axis and route \tilde{c} deviates from c -axis.

Noted that $\gamma^{(\text{top})}$ and $\gamma^{(\text{base})}$ correspond to the probabilities of that the vacancy found in a top (base) site after the vacancy wondering in a rep-site for a sufficiently long time.

Denoting the self-diffusion coefficients in direction a , c as $D(a)$, $D(c)$, the angle averaged self-diffusion coefficient of ε - Cu_3Ti -type domain can be evaluated as

$$D_{\text{Cu}_3\text{Ti}} = 1/3 \cdot (D(a) + D(c)). \quad (16)$$

Once the D_a^* and $D_{\tilde{c}}^*$ are obtained from eq. (2), they are projected into $D(a)$ and $D(\tilde{c})$ based on eq. (1):

$$D(a) = D_a^* + 2D_{\tilde{c}}^* \cos^2 \theta_{a\tilde{c}}, \quad (17)$$

$$D(c) = 2D_{\tilde{c}}^* \cos^2 \theta_{c\tilde{c}}. \quad (18)$$

Here, $\theta_{a\tilde{c}}$ ($\theta_{c\tilde{c}}$) is the angle between the direction a (c)-axis and route \tilde{c} .

FORMULA OF CORRELATION FACTOR

In order to obtain $D_{a,\tilde{c}}^*$ from eq. (2), we have to evaluate the correlation factors for both of the route a and route \tilde{c} . We established the equations alternating eq. (8) for multiple types of diffusion routes.

Before explaining about it, we will confirm the notation rules used in this paper. Suppose that the tracer (open cross) has just moved through route $l = a$ or \tilde{c} shown as the arrows towards the tracer in Fig. 6. The six sites surrounding the tracer are indexed with $k = 1 - 6$ in clockwise order beginning from the site where the tracer was positioned before moving. θ_k in eq. (5) is the angle between the directions of the sequential tracer moves. Hence, for example, $\theta_2 = \theta_{a\tilde{c}}$ for ion move $l = a$ and $\theta_2 = 2\theta_{c\tilde{c}}$ for ion move $l = \tilde{c}$. For convenience, the l dependency is noted as $\theta_k^{(l)}$ and a new function $L^{(l)}(k)$ is also introduced, which returns the type of the diffusion route (a or \tilde{c}) connecting site k and the tracer position. The return values are listed specifically as:

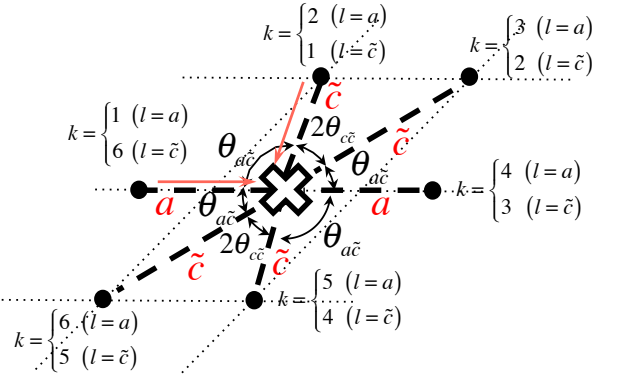


FIG. 6. The tracer just moved to the site denoted by open cross through route a or \tilde{c} . The surrounding 6 sites are indexed with $k = 1 \sim 6$ in a clockwise fashion beginning from the preceding tracer position before moving.

$L^{(a)}(k = 1, 4) = a$, $L^{(a)}(k = 2, 3, 5, 6) = \tilde{c}$, $L^{(\tilde{c})}(k = 3, 6) = a$, and $L^{(\tilde{c})}(k = 1, 2, 4, 5) = \tilde{c}$.

The n th-order average cosign $\langle \cos \theta \rangle_{l=a, \tilde{c}}^{(n)}$ may be built as the below recurrence formula similar to the idea for eq. (8):

$$\langle \cos \theta \rangle_{l=a, \tilde{c}}^{(n+1)} = \sum_k \frac{d_{L^{(l)}(k)}}{d_l} P_k^{(l)} \cdot \cos \theta_k^{(l)} \cdot \langle \cos \theta \rangle_{L^{(l)}(k)}^{(n)}. \quad (19)$$

This equation can be solved analytically and, of course, numerically also. The correlation factors for the ion jumps through route a and route \tilde{c} is given as same as eq. (6)

$$f_{a, \tilde{c}} = 1 + 2 \sum_{n=1}^{n_{\max}} \langle \cos \theta \rangle_{a, \tilde{c}}^{(n)} \approx 1 + 2 \sum_{n=1}^{\infty} \langle \cos \theta \rangle_{a, \tilde{c}}^{(n)}, \quad (20)$$

which is same as (6). Here, n_{\max} should be large enough for $f_{a, \tilde{c}}$ to be converged.

EVALUATION OF CORRELATION FACTOR

Before solving eq. (19) to obtain the average cosines $\langle \cos \theta \rangle_{l=a, \tilde{c}}^{(n)}$, $\{P_k^{(l)}\}$ should be prepared first, which represents the probability that the tracer gets pulled back by the vacancy from site k , after the tracer moved through route l . $\{P_k^{(l)}\}$ is given as the sum of the realization probabilities for the vacancy tracks pulling back the tracer from site k . This value can be reasonably approximated with considering only the vacancy tracks having highest realization probabilities. This is an example to obtain $\{P_k^{(l)}\}$: The tracer just moved to the central site (open cross) through the route a (double shafted arrow) in Fig. 7. Suppose that the vacancy moves through a route a , \tilde{c} with the selection probability $p_{a, \tilde{c}}$ (given later) and $\{P_k^{(l)}\}$ is given as the product of the ones of the routes included in the vacancy track. Thus, the realization probability becomes lower when the track consists of larger number of the diffusion routes in general. Now, we consider the two vacancy tracks shown as the red and blue arrows in Fig. 7. The former

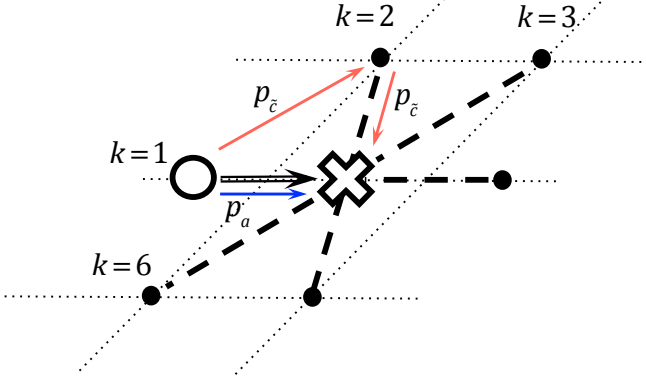


FIG. 7. An example of the vacancy tracks for jump $l = a$. The tracer is positioned at the central site (open cross) just after moving as the double shafted arrow. When considering the vacancy tracks including one or two routes, the vacancy tracks are limited in the ones shown by red and blues allows.

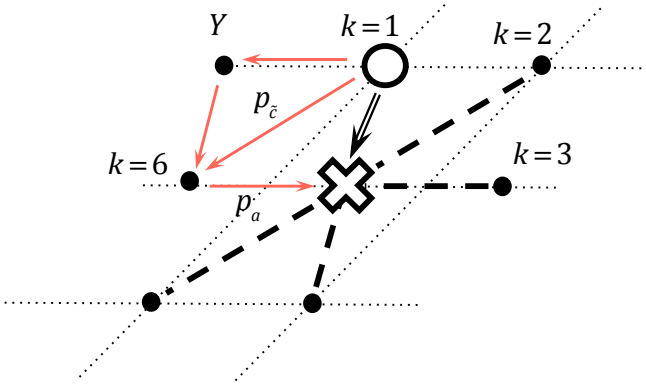


FIG. 8. An example of the vacancy tracks for jump $l = \tilde{a}$. The tracer is positioned at the central site (open cross) just after tracer moving as the double shafted arrow. The examples of the vacancy tracks are shown as the red arrows. The site Y is newly defined to take into account the vacancy tracks including the path from Y to 6.

consists of two routes \tilde{c} and the latter does of one route so the realization probabilities of the both tracks is given as $p_{\tilde{c}}^2$ and p_a respectively. Hence, $P_2^{(a)} = p_{\tilde{c}}^2 + p_a$.

$p_{a, \tilde{c}}$ is in proportion to $\eta_{a, \tilde{c}}(T)$ and given as

$$p_{a, \tilde{c}}(T) = \frac{\eta_{a, \tilde{c}}(T)}{2\eta_a(T) + 4\eta_{\tilde{c}}(T)}. \quad (21)$$

The denominator reflects that a rep-site connects to 2 rep-sites through route a and 4 rep-sites through route \tilde{c} . $p_{a, \tilde{c}}$ depends on temperature due to the Boltzmann factors in $\eta_{a, \tilde{c}}$, so the different vacancy tracks should be taken into account for different temperature. We considered the high and low temperature cases separately.

First, for the high temperature case, the relationship, $p_a \sim p_{\tilde{c}} \sim 1/6$ (e.g., $p_a/p_{\tilde{c}} = 1.03$ at $T=1000$ K), is given from *ab initio* calculations. Hence, $p_l = 17\%$, $p_l^2 = 3.8\%$, and $p_l^3 = 0.46\%$ so the vacancy tracks including 3 moves or more would be ignored. Then, the vacancy cannot pull back the tracer from site $k = 3 \sim 5$ for the preceding ion move through route $l = a$ and hence $P_{k=3 \sim 5}^{(a)} = 0$. The other $P_k^{(l=a)}$ are also straightforwardly given as $P_{k=1}^{(a)} = p_a$, $P_{k=2}^{(a)} = p_{\tilde{c}} \cdot p_{\tilde{c}}$, and $P_{k=6}^{(a)} = p_{\tilde{c}} \cdot p_{\tilde{c}}$. Applying the same analogy for $l = \tilde{c}$, $P_{k=3 \sim 5}^{(\tilde{c})}$ are zero and the others are $P_{k=1}^{(\tilde{c})} = p_{\tilde{c}}$, $P_{k=2}^{(\tilde{c})} = p_a \cdot p_{\tilde{c}}$, and $P_{k=6}^{(\tilde{c})} = p_{\tilde{c}} \cdot p_a$.

Secondly, for the low temperature case, p_a is much greater than $p_{\tilde{c}}$ (e.g., $p_a/p_{\tilde{c}} = 8.93$ at $T=300$ K). Thus, we suppose that, while the number of the vacancy moves through route \tilde{c} is limited in 0 or 1, that through route a is not limited. Then, we have to consider the infinite patterns of the vacancy tracks and it is apparently impossible. We introduced the following three tools to count up the primary vacancy tracks which have the high realization probabilities:

- Suppose to consider the vacancy tracks as the vacancy being finally at the starting site after the arbitrary n times of the vacancy moves through route a . The sum of the probabilities of the vacancy tracks is denoted by π_{even} .
- Suppose to consider the vacancy tracks as the vacancy being finally at the left (right) site of the starting site after the arbitrary n times of the vacancy moves. The sum of the probabilities of the vacancy tracks is denoted by π_{odd} .
- Suppose to consider the vacancy tracks as the vacancy being finally at the left (right) site of the starting site after the arbitrary $4n$ times of vacancy moves, imposing that the vacancy never gets into the sites positioned in the right (left) side from the starting site. The sum of the probabilities of the vacancy tracks is denoted as π_{oneside} .

Here, π_{even} and π_{oneside} must be greater than 1 because the vacancy has to be the starting site for $n = 0$. It is explained in the appendix how to deduce π_{even} , π_{odd} , and π_{oneside} .

$P_k^{(l)}$ is deduced here for every (k, l) using the three tools: (1) $l = a$, $k = 1$ case; We may consider the vacancy tracks that the vacancy roams in the left side from site $k = 1$ (including site $k = 1$) through route a before the pull-back. The probability sum [28] of the vacancy tracks before the pull-back from site $k = 1$ is exactly π_{oneside} . Hence, $P_{k=1}^{(a)} = \pi_{\text{oneside}} \cdot p_a$. (2) $l = a$, $k = 2 \sim 6$ case; Two vacancy moves through route \tilde{c} or more are required to pull back the tracer from these site. Hence, $P_{k=2 \sim 6}^{(a)} = 0$. (3) $l = \tilde{c}$, $k = 1$ case; We may consider the vacancy tracks that the vacancy roams through route a before the pull-back. The probability sum of the vacancy tracks before the pull-back from site $k = 1$ is exactly π_{even} . Hence, $P_{k=1}^{(\tilde{c})} = \pi_{\text{even}} p_{\tilde{c}}$. (4) $l = \tilde{c}$, $k = 2$ case; This case is quite similar to case (3). The difference is just that the vacancy pulls back

the tracer from the site $k = 2$ not $k = 1$ after roaming through route a . The probability sum just before the pull-back is exactly π_{odd} . Hence, $P_{k=2}^{(\tilde{c})} = \pi_{\text{odd}} p_c$. **(5)** $l = \tilde{c}$, $k = 3$ case; We may only consider such vacancy tracks that the vacancy moves to site $k = 2$ from $k = 3$. The probability sum before the vacancy positioned at site $k = 3$ is given as $\pi_{\text{odd}} p_c$ just like case (4), and that of the left vacancy tracks is given as $\pi_{\text{oneside}} p_a$ just like case (1). $P_{k=2}^{(\tilde{c})}$ is eventually given as the product of them: $P_{k=2}^{(\tilde{c})} = \pi_{\text{odd}} p_c \cdot \pi_{\text{oneside}} p_a$. **(6)** $l = \tilde{c}$, $k = 3 \sim 5$ case; Any of the vacancy tracks have to include two moves through route \tilde{c} or more. Hence, $P_{k=3 \sim 5}^{(\tilde{c})} = 0$. **(7)** $l = \tilde{c}$, $k = 6$ case; We may consider the two patterns of vacancy tracks before the vacancy positioned at the site $k = 6$: The vacancy moves to $k = 1$ from $k = 6$ or site Y (shown in Fig. 8). The probability sum before reaching site $k = 6$ is given as $(\pi_{\text{even}} + \pi_{\text{odd}}) p_{\tilde{c}}$, and that of the left vacancy tracks is equivalent to the one in case (1). $P_{k=6}^{(\tilde{c})}$ is eventually given as the product of them:

$$P_{k=6}^{(\tilde{c})} = (\pi_{\text{even}} + \pi_{\text{odd}}) p_{\tilde{c}} \cdot \pi_{\text{oneside}} p_a.$$

We discussed the high temperature and low temperature cases separately above. If considering the sum group of the vacancy tracks taken in the both cases to calculate the probability sums $P_k^{(l)}$, such $P_k^{(l)}$ may work well in the entire range of temperature. The vacancy tracks for the high temperature case are actually included in the ones of the low temperature case except for $l = \tilde{a}$, $k = 2, 6$. Eventually, $P_k^{(l)}$ is given as:

$$P_k^{(l)} = \begin{cases} \pi_{\text{oneside}} \cdot p_a & (l = a, k = 1) \\ p_{\tilde{c}}^2 & (l = a, k = 2, 6) \\ \pi_{\text{even}} \cdot p_{\tilde{c}} & (l = \tilde{c}, k = 1) \\ \pi_{\text{odd}} \cdot p_{\tilde{c}} & (l = \tilde{c}, k = 2) \\ \pi_{\text{odd}} \pi_{\text{oneside}} \cdot p_a p_{\tilde{c}} & (l = \tilde{c}, k = 3) \\ (\pi_{\text{even}} + \pi_{\text{odd}}) \pi_{\text{oneside}} \cdot p_a p_{\tilde{c}} & (l = \tilde{c}, k = 6) \\ 0 & (\text{otherwise}) \end{cases} \quad (22)$$

and eq. (19) becomes

$$\langle \cos \theta \rangle_a^{(n+1)} = -P_{k=1}^{(a)} \cdot \langle \cos \theta \rangle_a^{(n)} - 2 \cdot \frac{d_{\tilde{c}}}{d_a} \cdot P_{k=2,6}^{(a)} \cdot \cos \theta_{a\tilde{c}} \cdot \langle \cos \theta \rangle_c^{(n)}, \quad (23)$$

$$\langle \cos \theta \rangle_{\tilde{c}}^{(n+1)} = -\frac{d_a}{d_{\tilde{c}}} \cdot \left\{ P_{k=3}^{(\tilde{c})} \cdot \cos (2\theta_{c\tilde{c}} + \theta_{a\tilde{c}}) + P_{k=6}^{(\tilde{c})} \cdot \cos \theta_{a\tilde{c}} \right\} \cdot \langle \cos \theta \rangle_a^{(n)} - \left\{ P_{k=1}^{(\tilde{c})} - P_{k=2}^{(\tilde{c})} \cdot \cos 2\theta_{c\tilde{c}} \right\} \cdot \langle \cos \theta \rangle_{\tilde{c}}^{(n)}, \quad (24)$$

from which the n th-order average cosigns $\langle \cos \theta \rangle_{a,\tilde{c}}^{(n)}$ are given for any order n .

RESULTS AND DISCUSSION

Fig. 9 shows the convergence of f_a, \tilde{c} for n_{max} . f_a, \tilde{c} apparently vibrates for n_{max} because every pull-back denies the preceding tracer move. Further on, we consider only the converged values, which is actually used to solve the model.

If route a and \tilde{c} are equivalent, the coarse grained structure shown in Fig. 5 is regarded as ideal 2-dimensional hexagonal lattice. Its correlation factor is analytically known as 0.56[19] (shown as the dotted line in Fig. 9), so it is interesting to compare $f_{a,\tilde{c}}$ with the ideal value. First, in the case of low temperature ($T=300$ K), it is observed that f_a is lower and $f_{\tilde{c}}$ is higher than 0.56 respectively. This fact comes from that the vacancy moves through routes $l = a$ much more easily than through route $l = \tilde{c}$: The vacancy easily goes away from the tracer through route a after the tracer move $l = \tilde{c}$, so the pull-back seldomly happens and $f_{\tilde{c}}$ becomes higher. On the other hand, for the tracer move $l = a$, the vacancy moves through route a on the same line for many times, so the pull-back often happen and f_a becomes lower. In another way of thinking, the latter situation is similar to the 1-dim diffusion so f_a gets much lower. Secondly, in the case of high temperature ($T=1000$ K), it is expected that both f_a and $f_{\tilde{c}}$ converge

around 0.56 when temperature increasing, because route a and \tilde{c} are almost equivalent at high temperature and the diffusion network is similar to that on ideal 2-dim. hexagonal lattice. The converged values are actually higher than 0.56 by ~ 0.08 probably because of that the vacancy tracks including 3 routes and more are ignored, which can cause the overestimation of the self-diffusion coefficient. Nevertheless, the bias is quite small even at high temperature and presumably it should get less at low temperature because the number of the route a is not limited.

Once getting the correlation factors f_a, \tilde{c} , $D_{\text{Cu}_3\text{Ti}}$ can be calculated from eq. (16)~(18). Since $\varepsilon\text{-Cu}_3\text{Sn}$ phase consists of Cu_3Ti -type and D0_{19} -type domains with the ratio of $(M-2):2$, the self-diffusion coefficient in the phase is given as

$$D_{\varepsilon\text{-Cu}_3\text{Sn}} = \frac{M-2}{M} D_{\text{Cu}_3\text{Ti}} \quad (\because D_{\text{D0}_{19}} = 0). \quad (25)$$

The temperature dependency of $D_{\varepsilon\text{-Cu}_3\text{Sn}}$ is shown in Fig. 10 for both $M = 4$ and $M = \infty$. Although they have twice different values, the difference is relatively small compared with the scatter of the experimental values: Therefore, the experimental contradictions cannot be explained from the difference of periodicity M . It should be noted that the bias in the correlation factor f by ~ 0.08 is much smaller than the scatter. Our results look reproducing the experimental values reasonably as the predicted values pass though just the middle of the experimental values. On the other hand, the previous classical

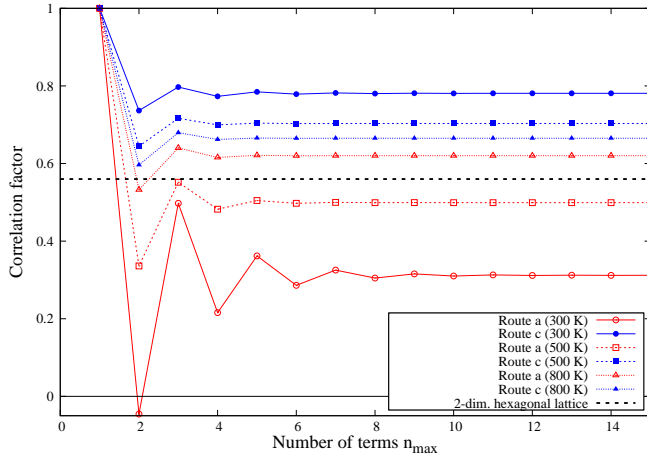


FIG. 9. The convergence of correlation factor f_a, \bar{c} for 300, 500, and 800 K evaluated from eq. (20). The black dotted line represents the correlation factor of 2-dimensional hexagonal lattice and the value is 0.56.[19].

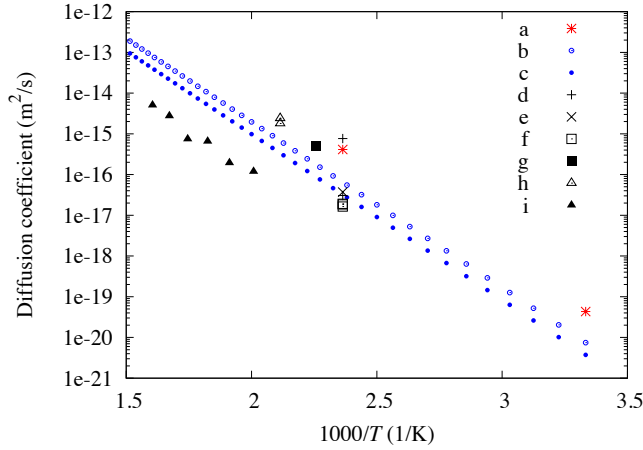


FIG. 10. a: Classical MD [18], b: This work ($M=\infty$), c: This work ($M=4$), d: Expt.[12], e: Expt.[13], f: Expt.[14], g: Expt.[15], h: Expt.[16], i: Expt.[17],

This graph compares our predictions for the diffusion coefficients (blue points) with the ones reported from the experiments (black points) and classical molecular dynamics (red points). The blue open (close) points correspond to the analysis with $M = \infty$, (4).

MD [18] overestimates our results by a digit. It is possible that the MD underestimated the potential top of diffusion route because of too large time step, since the time step is not shown in the previous paper.[18] However, usually the time step is femto-second order and it is sufficiently small compared with the time scale of the vibration shown in Tab. I. Hence, we tentatively conclude that the overestimation comes from the practical force-field, which is presumably less reliable especially for the description of the saddle point since three ions or more interact with the tracer.

SUMMARY AND PROSPECTS

We established a new modeling scheme for ion self-diffusion coefficient by introducing some novel concepts and formalisms. The scheme is applied to obtain the Cu self-diffusion coefficient in ε -Cu₃Sn phase of Cu-Sn alloy. The highlights are ‘domain division’ and ‘coarse graining’ of the diffusion network based on the barrier energies predicted by the *ab initio* calculation. In the former concept, the diffusion network is divided into the disjunct domains. Then, the calculation for the original large unitcell is replaced by the ones for the different types of simple domains, which significantly reduces the calculation cost. The diffusion network of our target system, ε -Cu₃Sn, is divided into the two types of domains, which have 1- and 2-dimensional networks respectively. It is concluded based on the textbook[19] that the former domain never contributes to the self-diffusion. In the latter concept, the diffusion network of each domain is coarse-grained by representing the ion sites with just a site, which are connected by the routes having the lowest barrier energies. This is on ground of that the vacancy moves through such routes much more easily than through the others. Eventually, it is significantly simplified to count up the vacancy tracks. After introducing the concepts, the model for ε -Cu₃Sn phase was successfully established and much better predictions by a digit than the previous classical MD study[18] in the comparison with the experimental values.

If the overestimation of self-diffusion coefficient in the previous classical MD work[18] comes from the usage of the practical potential, *ab initio* MD (AIMD) can be a strong competitor of our modeling scheme. Nevertheless, our scheme is superior to AIMD at the following points: First, the quantities included in the model can be evaluated from more reliable methods such as diffusion Monte Carlo method.[29] The merit is remarkable especially for such systems as transition metal dioxide[30, 31], where the severe accuracy is required to evaluate the electronic correlation effect. Secondly, it is challenging to evaluate the self-diffusion coefficient with AIMD in terms of the computational cost, because ion jump is a rare event. The recent attempt using the color-diffusion algorithm with non-equilibrium MD realizes more efficient simulation by increasing the rate of ion jumps.[32] Nevertheless, 1100 steps were used to obtain the self-diffusion coefficient in body centered molybdenum crystal at 1600 K. To make matters worse, more steps are required at lower temperature because ion jump occurs less frequently. The application of AIMD at low temperature is still challenging. On the other hand, while our scheme requires to construct the model by hand, the self-diffusion coefficient can be calculated with the reasonable cost. The merit becomes remarkable especially when performing a lot of similar calculations: For example, surveying how the additived ions affect the self-diffusion coefficient with modeling the inclusion of the additived ions using virtual crystal approximation.[33].

ACKNOWLEDGMENTS

The computation in this work has been performed using the facilities of the Research Center for Advanced Computing Infrastructure (RCACI) at JAIST. K.H. is grateful for financial support from a KAKENHI grant (JP17K17762), a Grant-in-Aid for Scientific Research on Innovative Areas “Mixed Anion” project (JP16H06439) from MEXT, PRESTO (JP-MJPR16NA) and the Materials research by Information Integration Initiative (MI²I) project of the Support Program for Starting Up Innovation Hub from Japan Science and Technology Agency (JST). R.M. is grateful for financial supports from MEXT-KAKENHI (17H05478 and 16KK0097), from Toyota Motor Corporation, from I-O DATA Foundation, and from the Air Force Office of Scientific Research (AFOSR-AOARD/FA2386-17-1-4049). R.M. and K.H. are also grateful to financial supports from MEXT-FLAGSHIP2020 (hp170269, hp170220).

APPENDIX

The probability sums π_{even} , π_{odd} , and π_{oneside} are deduced in the appendix. First, π_{even} corresponds to the probability sum of the following vacancy tracks: After $2n$ ($n = 0, 1, 2, \dots$) moves, the vacancy is positioned at the starting site. The realization probability of one of them is given as $p_a^{2n} \cdot (2n)! / (n!)^2$ and π_{even} is obtained by summing up them:

$$\pi_{\text{even}} = \sum_{n=0}^{\infty} p_a^{2n} \cdot (2n)! / (n!)^2. \quad (\text{i})$$

Secondly, π_{odd} corresponds to the probability sum of the following vacancy tracks: After $2n+1$ ($n = 0, 1, 2, \dots$) moves, the vacancy is positioned at the just right (left) site of the starting one. The realization probability of one of them is given as $p_a^{2n+1} \cdot (2n+1)! / n!(n+1)!$ and π_{odd} is obtain by summing up them:

$$\pi_{\text{odd}} = \sum_{n=0}^{\infty} p_a^{2n+1} \cdot (2n+1)! / n!(n+1)!. \quad (\text{ii})$$

Lastly, π_{oneside} corresponds to the probability sum of the following vacancy track: After $2n+1$ ($n = 0, 1, 2, \dots$) moves, the vacancy is positioned at the starting site with imposing that the vacancy never goes to the right (left) side of the starting site during moving. The total number of such tracks is given as the Catalan number[34]

$$c_n = \frac{1}{n+1} \frac{(2n)!}{(n!)^2}. \quad (\text{iii})$$

Thus, π_{oneside} is given as:

$$\pi_{\text{oneside}} = \sum_{n=0}^{\infty} c_n p_a^n. \quad (\text{iv})$$

- [1] G. Henkelman and H. J. nsson, The Journal of Chemical Physics **113**, 9978 (2000).
- [2] When the target ions are distributed ununiformly in the crystal, the distribution changes macroscopically with the thermal diffusion. This is called self-diffusion and the measure of the speed is self-diffusion coefficient.
- [3] W. Qiong, L. Shu-Suo, M. Yue, and G. Sheng-Kai, Chin. Phys. B **21**, 109102 (2012).
- [4] M. Mantina, Y. Wang, L. Chen, Z. Liu, and C. Wolverton, Acta Materialia **57**, 4102 (2009).
- [5] M. Mantina, S. L. Shang, Y. Wang, L. Q. Chen, and Z. K. Liu, Phys. Rev. B **80**, 184111 (2009).
- [6] S. Huang, D. L. Worthington, M. Asta, V. Ozolins, G. Ghosh, and P. K. Liaw, Acta Materialia **58**, 1982 (2010).
- [7] S. Choudhury, L. Barnard, J. Tucker, T. Allen, B. Wirth, M. Asta, and D. Morgan, Journal of Nuclear Materials **411**, 1 (2011).
- [8] X. Zhang, H. Deng, S. Xiao, Z. Zhang, J. Tang, L. Deng, and W. Hu, Journal of Alloys and Compounds **588**, 163 (2014).
- [9] A. D. Leclaire and A. B. Lidiard, The Philosophical Magazine: A Journal of Theoretical Experimental and Applied Physics **1**, 518 (1956), <https://doi.org/10.1080/14786435608238133>.
- [10] M. Koiwa and S. Ishioka, Philosophical Magazine A **48**, 1 (1983), <https://doi.org/10.1080/01418618308234882>.
- [11] M. Koiwa and S. Ishioka, Journal of Statistical Physics **30**, 477 (1983).
- [12] B. Chao, S.-H. Chae, X. Zhang, K.-H. Lu, M. Ding, J. Im, and P. S. Ho, Journal of Applied Physics **100**, 084909 (2006), <https://doi.org/10.1063/1.2359135>.
- [13] B. H.-L. Chao, X. Zhang, S.-H. Chae, and P. S. Ho, Microelectronics Reliability **49**, 253 (2009), recent Research Advances in Pb-free Solders.
- [14] Y. Yang, Y. Li, H. Lu, C. Yu, and J. Chen, Microelectronics Reliability **53**, 327 (2013), advances in Electrostatic Discharge (ESD) protection for ICs.
- [15] Y. Wang, S. H. Chae, J. Im, and P. S. Ho, in *2013 IEEE 63rd Electronic Components and Technology Conference* (2013) pp. 1953–1958.
- [16] S. Kumar, C. A. Handwerker, and M. A. Dayananda, Journal of Phase Equilibria and Diffusion **32**, 309 (2011).
- [17] A. Paul, C. Ghosh, and W. J. Boettinger, Metallurgical and Materials Transactions A **42**, 952 (2011).
- [18] F. Gao and J. Qu, Materials Letters **73**, 92 (2012).
- [19] H. Mehrer, “Diffusion in solids,” (Springer, 2007) Chap. Correlation in Solid-State Diffusion.
- [20] For example, if you consider the ion jumps between the sites having the shortest distance, there are only one type of diffusion routes. On the other hand, if you allow the ion jumps between the sites having the second shortest distance alos, there are two types of diffusion routes.
- [21] M. Van Sande, R. De Ridder, G. Van Tendeloo, J. Van Landuyt, and S. Amelinckx, physica status solidi (a) **48**, 383 (1978).
- [22] X. Sang, K. Du, and H. Ye, Journal of Alloys and Compounds **469**, 129 (2009).
- [23] K. Momma and F. Izumi, Journal of Applied Crystallography **44**, 1272 (2011).
- [24] G. Kresse and J. Furthmüller, Phys. Rev. B **54**, 11169 (1996).
- [25] H. Jónsson, G. Mills, and K. W. Jacobsen, “Nudged elastic band method for finding minimum energy paths of transitions,” in *Classical and Quantum Dynamics in Condensed Phase Simulations*, pp. 385–404.

- [26] J. P. Perdew, K. Burke, and M. Ernzerhof, Phys. Rev. Lett. **77**, 3865 (1996).
- [27] G. Kresse and D. Joubert, Phys. Rev. B **59**, 1758 (1999).
- [28] The sum of the probability for a group of vacancy tracks.
- [29] W. M. C. Foulkes, L. Mitas, R. J. Needs, and G. Rajagopal, Rev. Mod. Phys. **73**, 33 (2001).
- [30] Y. Luo, A. Benali, L. Shulenburger, J. T. Krogel, O. Heinonen, and P. R. C. Kent, New Journal of Physics **18**, 113049 (2016).
- [31] J. Trail, B. Monserrat, P. López Ríos, R. Maezono, and R. J. Needs, Phys. Rev. B **95**, 121108 (2017).
- [32] D. G. Sangiovanni, O. Hellman, B. Alling, and I. A. Abrikosov, Phys. Rev. B **93**, 094305 (2016).
- [33] L. Bellaiche and D. Vanderbilt, Phys. Rev. B **61**, 7877 (2000).
- [34] R. A. Monte, MIT Undergraduate Journal of Mathematics , 143 (1999).